International Journal for Numerical Methods in Fluids

WILEY

RESEARCH ARTICLE

Thermally Radiative Flow of Cattaneo–Christov Heat Flux in MHD Darcy–Forchheimer Micropolar Nanofluid With Activation Energy

Kakanuti Malleswari[1] | Jintu Mani Nath[2] | Mulinti Vinodkumar Reddy[1] | Kakarla Ramakrishna Reddy[3] | Bamdeb Dey[4]

[1]Department of Mathematics, Malla Reddy Engineering College (Autonomous), Secunderabad, India | [2]Department of Mathematics, Mangaldai College, Mangaldai, India | [3]Department of Mathematics, CMR Institute of Technology, Hyderabad, India | [4]Department of Mathematics, Assam Don Bosco University, Guwahati, Assam, India

Correspondence: Bamdeb Dey (bamdebdey88@gmail.com)

Received: 3 May 2025 | **Revised:** 9 May 2025 | **Accepted:** 19 June 2025

Funding: The authors received no specific funding for this work.

Keywords: activation energy | Cattaneo–Christov heat flux | chemical reaction | Darcy–Forchheimer | heat source | micropolar fluid | nanofluid | thermal radiation

ABSTRACT

The present inquiry examines the necessity for enhanced thermal transfer approaches across multiple industrial domains, such as energy generation and processing of materials, through an investigation of the intricate dynamics of micropolar nanofluids. The main objective is to numerically simulate the Cattaneo–Christov heat flux in magnetohydrodynamics (MHD) to investigate the radiative behavior of Darcy–Forchheimer micropolar nanofluids, including the effects of activation energy. The study presumes steady-state conditions and employs particular constitutive equations to characterize the behavior of the nanofluid. The governing equations, which incorporate binary chemical interactions, radiation, and a thermal source, are reformulated with similarity variables into a system of nonlinear ordinary differential equations (ODEs). The BVP4C MATLAB software is utilized for obtaining numerical solutions. The study indicates that an increase in thermophoresis, thermal source, radiation, and Brownian motion factors improves thermal distributions in micropolar nanofluid flow. Moreover, increased radiation parameters result in a rise in the thermal transmission rate, while enhancing activation energy factors leads to a decrease. The findings are essential for enhancing temperature control in systems and for the development of efficient thermal appliances.

1 | Introduction

The efficacy of heat transmission inside a system is measured by the thermal transport rate. The heightened convective heat transfer capabilities and higher thermal conductivity of nanofluids (fluids incorporating nanoparticles) allow them to improve this rate. In light of this, nanofluids are suitable for purposes involving nuclear reactor cooling systems, automobile engines, and electronics cooling systems where effective heat dissipation is crucial. In view of this, the consequences of thermal energy and buoyancy on the motion of MHD micropolar nanofluids were computationally calculated by Rehman et al. [1] via an elongating/shrinking sheet incorporating the thermal source. Moreover, Alqahtani et al. [2] examined the thermal analysis of a radiative nanofluid across an extending/shrinking cylinder integrating viscous dissipation. Also, Ullah et al. [3] examined the conjugate heat transmission of simultaneous convection and entropy production of nanofluid under an external magnetic field using a computational technique, noting that the thermal conductivity levels of the material were systematically adjusted from 0.2 to 5. Majeed et al. [4] in their work quantitatively investigated all potential strategies to optimize heat transfer in a sinusoidal cavity using oxide nanoparticle dispersion in fluid. Recently, a few researchers [5–7] have contributed their significant exploration of the field of nanofluids.

The study of unconventional fluid mechanics has garnered considerable academic interest owing to its expanding importance in the organization and industrial sectors. Shear force dependency and shear rate are connected to the distinctive features and geometry of non-Newtonian fluids. Colorants, mixed materials, coverings, polymeric solutions, wastewater effluent, clay-based concrete, and pharmaceutical compounds are a few examples of notable applications for non-Newtonian substances. Non-Newtonian fluid behavior is displayed by several kinds of biological fluids, including blood, saliva, and synovial fluid. For non-Newtonian fluids, there are a number of well-established models that capture their characteristics. One such model is the micropolar fluid paradigm; it incorporates an extensive spectrum of distinct characteristics and technical applications, encompassing animal blood, liquid crystals, and polymeric suspensions. Their classification encompasses an enormous scope of investigation. To recognize this, Hayat et al. [8] analyzed the steady movement of a mixed convective micropolar fluid past a nonlinear elongating surface via the homotopy analysis approach. The hydromagnetic flow of chemically reacting micropolar nano liquid via an expanding sheet was thought of by Dawar et al. [9]. Awan et al. [10] integrated the effects of electrical magnetohydrodynamics (MHD) and Hall current into a computational study of the flow of micropolar nanofluids between a configuration of parallel plates. Moreover, recent studies on non-Newtonian fluid motion are illustrated in Refs. [11–13].

Fluid flow through porous media is described by the Darcy–Forchheimer model, which takes into account both Forchheimer's correction for high-velocity, nonlinear flow and Darcy's law, which controls slow, linear flow. For the purpose of precisely forecasting pressure drops and flow rates in porous materials, this model is indispensable. Applications include groundwater hydrology for aquifer investigation, chemical engineering for packing bed reactor design, and petroleum engineering for the simulation of reservoirs. In view of this, Rahman et al. [14] analyzed the viscous nanomaterial movement integrating Darcy–Forchheimer and activation energy. Moreover, Bafe et al. [15] investigated with an exponentially expanded surface the MHD thermo-bioconvective motion of a spinning Williamson nanofluid, including Arrhenius stimulation energy in a Darcy–Forchheimer medium. As an additional source, Ali et al. [16] discussed the wave variations in the Darcy–Forchheimer nanofluid stream using a buoyancy-based permeable surface in the thermal boundary barrier. In a recent study, Al-Shammari et al. [17] investigated the effects of activation and thermal transmission on the oscillatory thermo-mass transmission of Darcy–Forchheimer tiny fluids with a cone that produces heat.

The study of MHD addresses how electrically conducting fluids behave while magnetic fields are introduced. MHD studies heat transport and energy loss in fluids in conjunction with thermal radiation, viscous dissipation, and heat sources. This holds significant importance in the design of cooling systems for nuclear reactors, heat control in spacecraft, and material handling in metallurgy. In light of this, Sharma and Gandhi [18] scrutinized the MHD flow rate within a vertically extending plate situated in a Darcy–Forchheimer porous medium, focusing on the synergistic effects of Joule heating and a non-uniform thermal source/sink. Furthermore, Hasanuzzaman et al. [19] studied the effects of fluid dissipation on the transient magneto-convective thermo-mass transmission on a vertical permeable surface that incorporates thermal radiation. Using an expanding sheet, Alamirew et al. [20] investigated the influences of Hall effect, ion slip, viscous dispersion, and asymmetric radiant heat on the dynamics of MHD Williamson nanofluids. The researchers [21, 22] have investigated the MHD fluid flow under different circumstances.

One effective model of the process for transferring heat is Fourier's law for conduction of heat. The Fourier's model was further developed by Cattaneo [23] in 1948 by adding a thermal relaxation time. Thermal relaxation durations, however, vary throughout materials. With this in mind, Christov [24] created the Cattaneo–Christov heat flow model, a time derivative model. For convective heat transport investigation, this model is quite significant. In systems like micro and nanotechnology, high-speed heat imaging, and thermal-sensitive biological tissues, where rapid thermal reactions take place, this paradigm is essential. Ibrahim and Gadisa [25] conducted a simulation of the computational results for the nonlinear convective motion of Oldroyd-B fluid using the Cattaneo–Christov thermal flux scheme. In addition, Waqas et al. [26] conducted a computer simulation to analyze the generation of entropy in a nanofluid, considering the effects of thermal radiation and the Cattaneo–Christov heat flow model. Ashraf et al. [27] investigated the effects of Cattaneo–Christov heat flux on the flow of MHD Jeffery nanofluid around a stretched cylinder. Azam et al. [28] studied nanofluid flow on a surface that moves in two directions. The study focused on the Darcy–Forchheimer area and included the Cattaneo–Christov thermal flux. Recently, Karthik et al. [29] numerically simulated the MHD fluid movement incorporating thermal sink using the Cattaneo–Christov source.

The energy at which a reactant molecule turns into a product is known as activation energy, and it is a key idea in chemical kinetics. It was first applied by Svante Arrhenius to control reaction kinetics and explain the energy barrier for reaction initiation. Hyperthermia, which maximizes cell death induction temperatures through the use of dosimetry, is crucial to the treatment of cancer. Along with medicine formulation and stability testing, it is important for food preservation. In the flow of Prandtl–Eyring nanofluid, Khan et al. [30] assessed the optimization of entropy creation using the dual chemical process and the Arrhenius activation energy. Moreover, Ram et al. [31] included the effect of activation energy in computational simulations of magneto micropolar fluid stagnation region movement across a stretchable surface. Also, Salahuddin et al. [32] investigated the significance of an MHD cross-nanofluid investigation close to a surface integrating dual stratification and activation energy. Recently, Ali et al. [33] investigated the activation energy effects included in the unsteady convective electro-periodic MHD flow via a stretching sheet.

1.1 | Novelty of the Study

This research is the first of its kind to integrate activation energy, heat production, a radiation source, a binary chemical reaction, and the Cattaneo–Christov heat flux model with MHD radiative flow in a Darcy–Forchheimer micropolar nanofluid. Thermophoresis and Brownian motion are assessed in detail using the Buongiorno nanofluid model. By integrating many physical phenomena and focusing on this particular form of nanofluid, we fill a significant knowledge vacuum and provide useful insights for improving heat management systems in various engineering contexts. Understanding the interplay between Lorentz forces and buoyancy-driven motions, as well as radiation and chemical effects, is essential for optimizing applications ranging from coating processes to microfluidic devices.

Computational solutions for velocity, microrotation, mass, and temperature profiles, together with skin friction, coupled stress, and rates of heat and mass transfer, are derived using the MATLAB BVP4C technique. This study provides essential insights for improving heat management systems in many technical applications, such as electronic device cooling, thermal exchanger efficiency, and energy system optimization. By clarifying the intricate fluid dynamics of micropolar nanofluids, engineers may develop advanced thermal systems with enhanced efficiency and effectiveness, leading to improved performance and energy conservation in industrial and technical operations. This study establishes a solid groundwork for future inquiries and developments in sustainable energy technologies and thermal control systems by pinpointing essential parameters such as the thermal relaxation parameter and suction effects.

2 | Mathematical Formulation

Attempt to examine a situation where the fluid is stable and incompressible. The study is on the behavior of Darcy–Forchheimer Micropolar nanomaterial in an MHD convective flow towards an extended sheet in a permeable medium. To characterize the event, the Cattaneo–Christov hypothesis is executed. Radiation, a heating source, and a binary chemical interaction are also included. The Buongiorno nanofluid model is used to evaluate the characteristics of Brownian motion and thermophoresis. For the purpose of simulating the study, the coordinates (x, y) have been taken into consideration. The x-axis represents the sheet in fluid flow, while the y-axis is normal to the sheet and represents its velocity as u_w. An intense uniform magnetic field B_0 is issued in y-direction and perpendicular to the direction of flow. The consistent and ambient temperature, alongside the levels of concentrations are T_w, T_∞, C_w, and C_∞, respectively. In Figure 1, the flow phenomenon is illustrated. Under the limit layer considerations and assumptions, the fluid flow equations are:

$$\frac{\partial u}{\partial x} + \frac{\partial v}{\partial y} = 0 \tag{1}$$

$$u\frac{\partial u}{\partial x} + v\frac{\partial u}{\partial y} = \left(\frac{\mu + k}{\rho}\right)\frac{\partial^2 u}{\partial y^2} + \left(\frac{k}{\rho}\right)\frac{\partial N}{\partial y} - \frac{\sigma\beta_0^2 u}{\rho} - \frac{\mu}{\rho k_1}u + g\beta_T(T - T_\infty) + g\beta_C(C - C_\infty) - \frac{c_b}{\sqrt{k_1}}u^2 \tag{2}$$

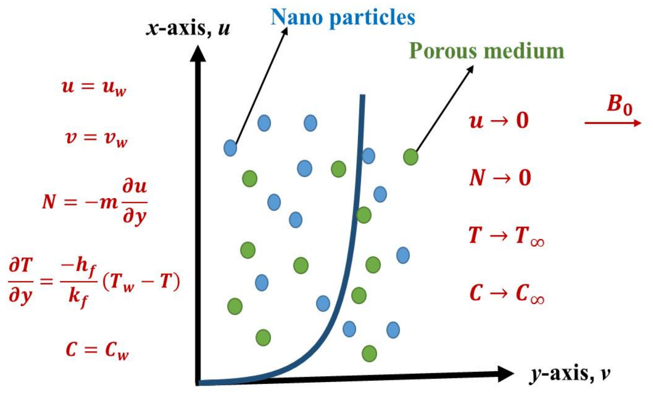

FIGURE 1 | Geometrical view of flow problem. [Colour figure can be viewed at wileyonlinelibrary.com]

$$\left(u\frac{\partial N}{\partial x} + v\frac{\partial N}{\partial y}\right) = \left(\frac{\gamma^*}{\rho j}\right)\frac{\partial^2 N}{\partial y^2} - \left(\frac{k}{\rho j}\right)\left(2N + \frac{\partial u}{\partial y}\right) \tag{3}$$

$$\begin{aligned} u\frac{\partial T}{\partial x} + v\frac{\partial T}{\partial y} &= \alpha\frac{\partial^2 T}{\partial y^2} + \left(\frac{\mu + k}{\rho C_P}\right)\left(\frac{\partial u}{\partial y}\right)^2 \\ &+ \tau\left(D_B\frac{\partial c}{\partial y}\frac{\partial T}{\partial y} + \frac{D_T}{T_\infty}\left(\frac{\partial T}{\partial y}\right)^2\right) \\ &- \frac{1}{\rho C_P}\frac{\partial q_r}{\partial y} + \frac{Q_o}{\rho C_P}(T - T_\infty) \\ &- \lambda\left[u\frac{\partial u}{\partial x}\frac{\partial T}{\partial x} + v\frac{\partial v}{\partial y}\frac{\partial T}{\partial y} + u\frac{\partial v}{\partial x}\frac{\partial T}{\partial y} + v\frac{\partial u}{\partial y}\frac{\partial T}{\partial x} \right.\\ &\left. + 2uv\frac{\partial^2 T}{\partial x \partial y} + u^2\frac{\partial^2 T}{\partial x^2} + v^2\frac{\partial^2 T}{\partial y^2}\right] \end{aligned} \tag{4}$$

$$\begin{aligned} u\frac{\partial C}{\partial x} + v\frac{\partial C}{\partial y} &= D_B\frac{\partial^2 C}{\partial y^2} + \frac{D_T}{T_\infty}\frac{\partial^2 T}{\partial y^2} \\ &- K_r^2(C - C_\infty)\left(\frac{T}{T_\infty}\right)^n exp\left(\frac{-E_a}{kT}\right) \end{aligned} \tag{5}$$

The appropriate boundary conditions are as follows:

$$\begin{aligned} &u = u_w, v = v_w, N = -m\frac{\partial u}{\partial y}, \frac{\partial T}{\partial y} = \frac{-h_f}{k_f}(T_w - T), C = C_w \ at \ y = 0, \\ &u \to 0, N \to 0, T \to T_\infty, C \to C_\infty \quad as \quad y \to \infty \end{aligned} \tag{6}$$

In this context, u and v represent velocities in the x and y directions, respectively, ρ is the density, k_1 is the media's porosity coefficient, α is the thermal diffusivity, q_r is the radiative heat flux, $Q_\circ$ is the heat source/sink coefficient, and K_r is the chemical reaction rate, respectively.

Introducing the similarity transformations as:

$$\begin{aligned} &u = bxf'(\eta), v = -(b\vartheta)^{\frac{1}{2}}\ f(\eta), N = bx\sqrt{\frac{b}{\vartheta}}\ , \eta = \sqrt{\frac{b}{\vartheta}}\ y, \\ &\theta(\eta)(T_w - T_\infty) = T - T_\infty, \phi(\eta)(C_w - C_\infty) = C - C_\infty \end{aligned} \tag{7}$$

By applying the similarity transformations in Equations (2–7), we obtained the following dimensionless equations:

$$(1+K)f''' + ff'' + Kg' - (M+K_P)f' + \lambda_1\theta + \lambda_2\phi - Frf'^2 - f'^2 = 0 \quad (8)$$

$$\left(1+\frac{K}{2}\right)g'' + fg' - f'g - K(2g+f'') = 0 \quad (9)$$

$$\left((1+R) - Pr\delta f^2\right)\theta'' + Pr\begin{bmatrix} f\theta' - \delta f f'\theta' + Nb\theta'\phi' + Nt\theta'^2 + Q\theta \\ +(1+K)Ecf''^2 \end{bmatrix} = 0 \quad (10)$$

$$\phi'' + Scf\phi' + \frac{Nt}{Nb}\theta'' - Sc\gamma(1+\alpha_1\theta)^n exp\left(\frac{-E}{1+\alpha_1\theta}\right)\phi = 0 \quad (11)$$

The corresponding boundary conditions are:

$$f(0) = s, f'(0) = 1, g(0) = -mf''(0), \theta(0) = 1, \phi(0) = 1,$$
$$f'(\infty) = 0, g(\infty) = 0, \theta(\infty) = 0, \phi(\infty) = 0 \quad (12)$$

where,

$$M = \frac{\sigma B_\circ^2}{\rho b}, K_p = \frac{\upsilon}{bk_1}, K = \frac{k}{\rho\upsilon}, \lambda_1 = \frac{g\beta_T(T_w - T_\infty)}{b^2 x},$$
$$\lambda_2 = \frac{g\beta_C(C_w - C_\infty)}{b^2 x}, \delta = b\lambda, R = \frac{16\sigma^* T_\infty^3}{3k^* k}, Pr = \frac{\upsilon}{\alpha},$$
$$Q = \frac{Q_\circ}{\rho C_p b}, Ec = \frac{u_w^2}{(T_w - T_\infty)C_p}, Nb = \frac{\tau D_B(C_w - C_\infty)}{\upsilon},$$
$$Nt = \frac{\tau D_T(T_w - T_\infty)}{T_\infty \upsilon}, Sc = \frac{\upsilon}{D_B}, \ \gamma = \frac{K_r^2}{b}, E = \frac{E_a}{kT_\infty}, S = -\frac{\upsilon_w}{\sqrt{b\upsilon}} \quad (13)$$

The physical variables are demonstrated as follows:

$$C_f(Re)^{0.5} = 2(1 + K(1-m))f''(0), \ \ C_S(Re)^{0.5} = \left(1+\frac{K}{2}\right)g'(0),$$
$$Nu(Re)^{-0.5} = -(1+R)\theta'(0), \ \ Sh(Re)^{-0.5} = -\phi'(0) \quad (14)$$

3 | Solution

The transformed Equations (8–11) alongside the boundary limitations (12) are numerically solved using the bvp4c MATLAB program using a shooting approach. By taking into account certain variables, this approach converts higher-order nonlinear ordinary differential equations (ODEs) into first-order ODEs. The considered variables as $T_1 = f, T_2 = f', \ T_3 = f'', \ T_4 = g, T_5 = g', \ T_6 = \theta, T_7 = \theta' \ \ T_8 = \phi, \ \ T_9 = \phi'$. Then, the first-order ODEs are expressed as follows:

$$f' = \ T_2 \quad (15)$$

$$f'' = \ T_3 \quad (16)$$

$$T_3' = \left(\frac{1}{(1+K)}\right)\left[(M+K_P)\,T_2 - T_1T_3 - K\,T_5 - \lambda_1\,T_6 - \lambda_2\,T_8 + FrT_2\,T_2 + T_2\,T_2\right] \quad (17)$$

$$g' = \ T_5 \quad (18)$$

$$T_5' = \frac{1}{\left(1+\frac{K}{2}\right)}\left[\,T_2\,T_4 - T_1T_5 + K(2T_4 + T_3)\right] \quad (19)$$

$$\theta' = T_7 \quad (20)$$

$$T_7' = \frac{1}{[(1+R) - Pr\delta T_1T_1]}\Big(Pr\big[\delta T_1T_2\ T_7 - T_1\ T_7 - Q\ T_6$$
$$-Nb\ T_7\ T_9 - Nt\ T_7\ T_7 - (1+K)Ec\ T_3T_3\big]\Big) \quad (21)$$

$$\phi' = T_9 \quad (22)$$

$$T_9' = -\frac{Nt}{Nb}\Bigg[\frac{1}{[(1+R) - Pr\delta T_1T_1]}\Big(Pr\big[\delta T_1T_2T_7 - T_1\ T_7 - Q\ T_6$$
$$-Nb\ T_7\,T_9 - Nt\,T_7\,T_7 - (1+K)Ec\ T_3T_3\big]\Big)\Bigg]$$
$$-\ ScT_1\,T_9 + Sc\gamma(1+\alpha_1T_6)^m exp\left(\frac{-E}{1+\alpha_1T_6}\right)T_8 \quad (23)$$

Along with boundary conditions

$$T_1(0) = S, T_2(0) = 1, \ \ T_4(0) = -mT_3, \ \ T_6(0) = 1, T_8(0) = 1 \ at\ \eta = 0,$$
$$T_2(\infty) = 0, \ \ T_4(\infty) = 0, \ \ T_6(\infty) = 0, T_8(\infty) = 0 \ \ as \ \ \eta \to \infty \quad (24)$$

4 | Results and Discussion

An analysis of the behavior of the Cattaneo–Christov model in the context of the MHD radiant circulation by Darcy–Forchheimer is being conducted. An investigation was conducted on the conveyance of micropolar nanofluid through a porous media to analyze the effects of heat radiation, chemical interactions, and energy stimulation, taking into account the consequences of magnetism and suction. In the current study, the nonlinear PDEs (2–5) are first converted into a set of associated ODEs (8–11) by the use of similarity variations. The final outcomes were solved numerically via the bvp4c MATLAB. For this analysis, the fixed parameter values are as $M = 0.5$, $K_p = 0.1$, $K = 0.2$, $Fr = 0.3$, $\lambda_1 = 0.1$, $\lambda_2 = 0.1$, $Nb = 0.2$, $Nt = 0.2$, $Sc = 0.5$, $Q = 0.2$, $\gamma = 0.5$, $Pr = 0.72$, $R = 0.5$, $Ec = 0.1$, $E = 0.5$, and $S = 0.1$.

Figure 2a–h depicts velocity curves for different constraint parameters. Figure 2a shows the significant effect of the magnetic variable (M) on the velocity fields. Figure 2a demonstrates that there is a reduction in flow rate as M increases. As the value of M grows, a restrictive force occurs inside the computing domain. The term "restriction force" is synonymous with the Lorentz force. The Lorentz force functions as a barrier that reduces the fluid velocity. The value of K in micropolar fluids reflects the impact of micro-rotation. As the value of K grows, it strengthens the connection among micro-rotational and axial movement, resulting in a decrease in viscous stiffness and enabling the medium to travel with more grace, ultimately leading to a gain in the flow rate, as shown in Figure 2b. Figure 2c,d shows that, when the porosity parameter K_p and the Darcy–Forchheimer Fr both raises, the velocity decreases. This occurs due to the enhanced medium's porosity, which enables a greater amount of

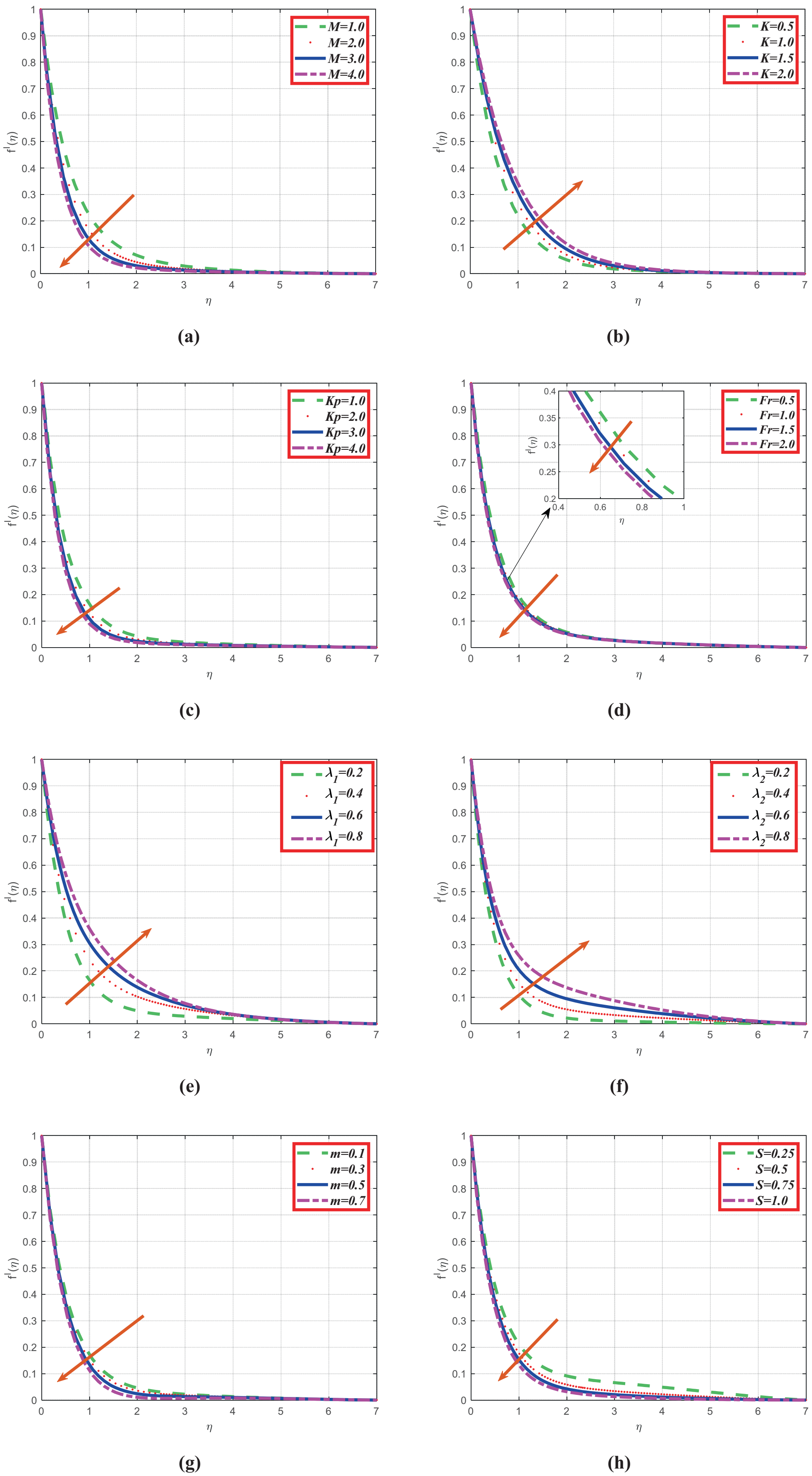

FIGURE 2 | (a–h) Variation of the M, K, K_p, Fr, λ_1, λ_2, m, and S on the $f'(\eta)$. [Colour figure can be viewed at wileyonlinelibrary.com]

fluid to permeate, hence decreasing the velocity of the stream. The Darcy–Forchheimer phenomenon considers the combined resistance of viscosity and momentum in porous materials, resulting in a greater drag and thus a further reduction in fluid velocity. The implications described have practical applications in several fields, such as mineral engineering, subterranean hydrology, and mechanical engineering. The distribution of velocity shown in Figure 2e,f demonstrates a direct correlation with the thermal Grashof number and the solutal Grashof number. These values signify the buoyant forces resulting from variations in heat and concentration, respectively. The velocity gradient grows as the boundary parameter m rises, as seen in Figure 2g. Figure 2h shows that when the suction parameter S increases, the flow rate at the surface reduces due to the removal of fluid from the frontier layer, which thins it. Consequently, the velocity distribution drops.

The microrotation profile for various constraint settings is shown in Figure 3a–h. The microrotation contour rises in proportion to the magnetism owing to intensified Lorentz forces, resulting in an amplified transmission of axial momentum inside the nanofluid, as seen in Figure 3a. This leads to enhanced rotational movement of the fluid's tiny particles, thereby raising the microrotation profile. The microrotation characteristic diminishes, as observed in Figure 3b, when the micropolar fluid variables rise due to the heightened resistance to the microrotation of molecules of fluid caused by these factors, such as the interaction factor and spin viscosity. This increased resistance mitigates the rotational impacts, resulting in a decrease in the microrotation gradient. Optimizing these characteristics is essential in applications such as coating, biomedical research, and polymer synthesis. The microrotation contour exhibits an upward trend as the permeability metrics and the Darcy–Forchheimer parameter rise. This is attributed to the enhanced interaction between the medium's fluid and the porous medium, as seen in Figure 3c. Since both the thermal Grashof number and the solutal Grashof number reflect the buoyant forces caused by temperature and concentration variations, respectively, a rise in either of these values causes the microrotation pattern to diminish, which can be seen in Figure 3e,f. The proportional impact of microrotation is reduced and buoyancy-driven motions take over when the Grashof number is significant. Consequently, there is a decrease in the angular momentum of the fluid's nanoparticles. Natural convection mechanisms, such as airflows and thermal exchangers, rely on this behavior. The shear forces and fluid-boundary coupling are both amplified as m rises, leading to increased spin of fluid particles close to the barrier. Figure 3g shows the enhanced microrotation gradient that follows from this. Applications such as microfluidics and streamlined material design greatly benefit from these effects. As shown in Figure 3h, the microrotation contour diminishes when the suction variable grows. This occurs because, when the Hoover removes fluid particles from the outermost layer, the overall amount of flow at the surface diminishes.

The temperature gradient for different constraint configurations is portrayed in Figure 4a–i. In recognition of the field's magnetic effect on flow mechanics, micropolar tiny fluids' temperature profiles rise with magnetism parameters. As the magnetic characteristic rises, the magnetic field's Lorentz force opposes flow, increasing viscosity and energy transformation. This radiation raises the fluid temperature. Furthermore, the magnetic gradient has an impact on the microstructure and tilting behavior of the micropolar fluid. This, in turn, impacts its thermal transit characteristics, increasing the temperature spectrum as seen in Figure 4a. The thermal relaxation parameter δ quantifies the delay in the passage of thermal radiation. A higher thermal relaxation parameter leads to a longer duration for the fluid to adapt to temperature variations, yielding a more efficient outcome dispersion of heat and, therefore, a reduction in the entire temperature characteristics, as seen in Figure 4b. Increased thermal and solutal Grashof counts improve buoyancy-driven flow in micropolar nanofluids, improving thermal and mass transmission. Enhanced convection better reorganizes heat energy, lessening variations in temperature and gradient. In Figure 4c,d, greater convective forces diffuse heat more evenly, lowering the temperature description. Figure 4e,f shows that nanoparticle mechanics raise the thermal distribution in micropolar nanofluids with increased Brownian motion and thermophoresis properties. Brownian motion lets nanoparticles diffuse quickly by thermal arousal, whereas thermophoresis causes variations in temperature displacement. These events increase nanofluid thermal efficiency. The increased conductivity enhances energy transmission efficiency, raising the temperature spectrum. This behavior matters in sophisticated radiators and thermal exchangers. Due to energy intake and heat transmission, heat source and radiation factors raise the temperature profile. Figure 4g shows that a higher heat source value heats the fluid. Figure 4h shows that rising radiation parameters intensify fluid radiant energy, causing greater absorption. These actions enhance fluid heat, raising its temperature. Augmenting suction parameters improves the extraction of fluid from the boundary layer, hence decreasing heated edge layer thickness. The enhanced suction leads to a decrease in thermal distribution, depicted in Figure 4i, by facilitating improved heat dissipation and minimizing the occurrence of localized heating near the surface.

The concentration profile for various restriction setups is shown in Figure 5a–e. Optimized Brownian motion accelerates the diffusion of nanoparticles, resulting in a decrease in concentration distributions. The heightened dispersal leads to a more homogeneous scattering of nanoparticles, resulting in a decreased concentration gradient (Figure 5a). This occurs when the particles disperse more uniformly within the fluid. As shown in Figure 5b, increased thermophoresis raises the concentration distribution. Thermophoresis propels nanoparticles to lower temperatures, where they accumulate. This controlled movement increases nanoparticle concentration in colder locations, raising the concentration gradient as particles transit and consolidate. Increased activation energy factor E inhibits nanoparticle-consuming chemical processes, increasing concentration depicted in Figure 5c. Larger activation energy requires an elevated thermal energy barrier for responses, reducing nanoparticle depletion. A higher Schmidt number, which quantifies the relationship between the diffusion of momentum and the diffusion of mass, leads to a reduced concentration distribution. Higher Schmidt numbers correspond to decreased mass diffusivity, resulting in a slower diffusion rate for nanoparticles as seen in Figure 5d. An augmentation in chemical reaction settings expedites the depletion of nanoparticles via chemical interactions. The accelerated procedure results in a faster depletion of nanoparticles, resulting in a decrease in the concentration gradient illustrated in Figure 5e. This behavior is very necessary in

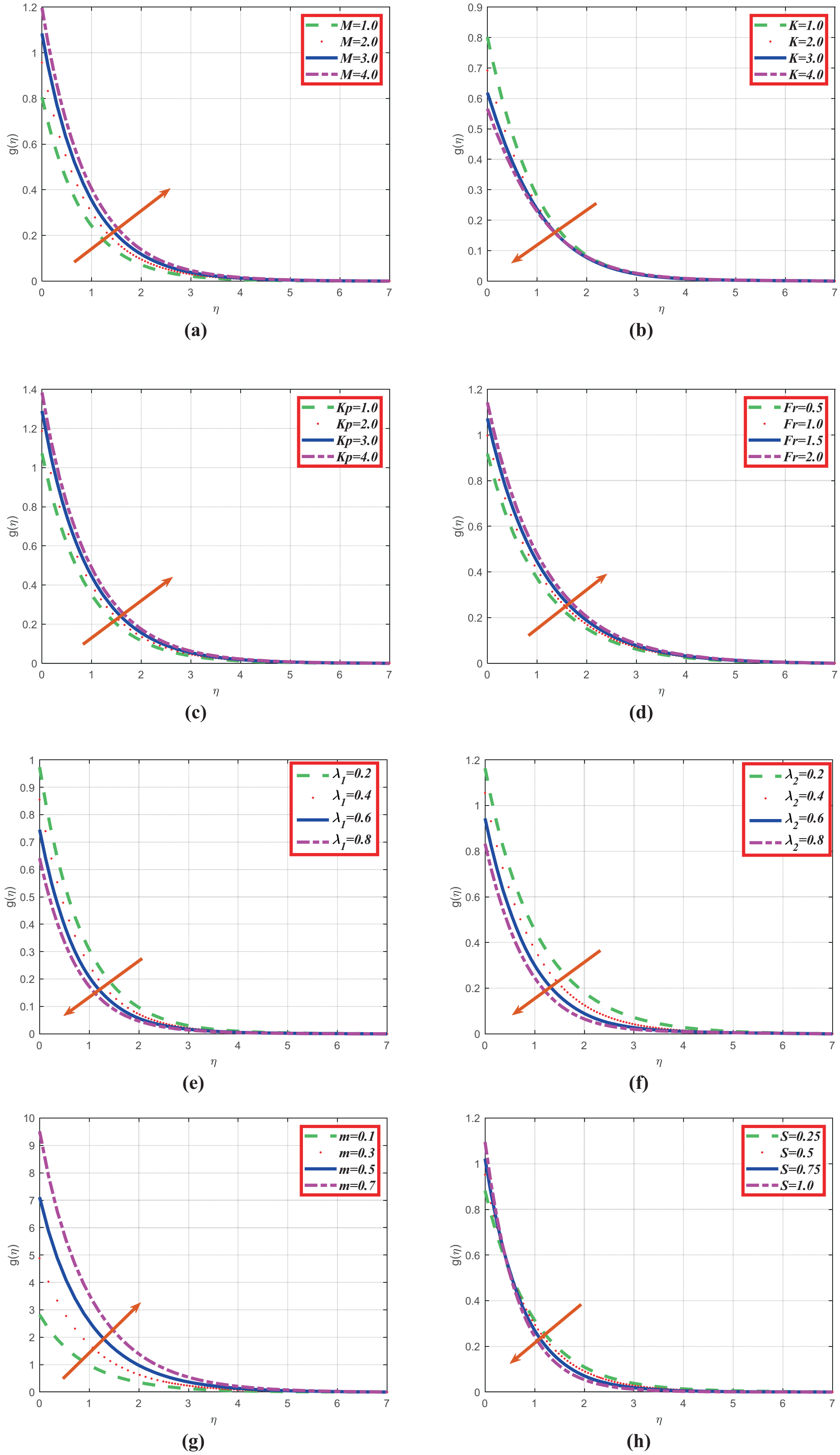

FIGURE 3 | (a–h) Variation of the M, K, K_p, Fr, λ_1, λ_2, m, and S on the $g(\eta)$. [Colour figure can be viewed at wileyonlinelibrary.com]

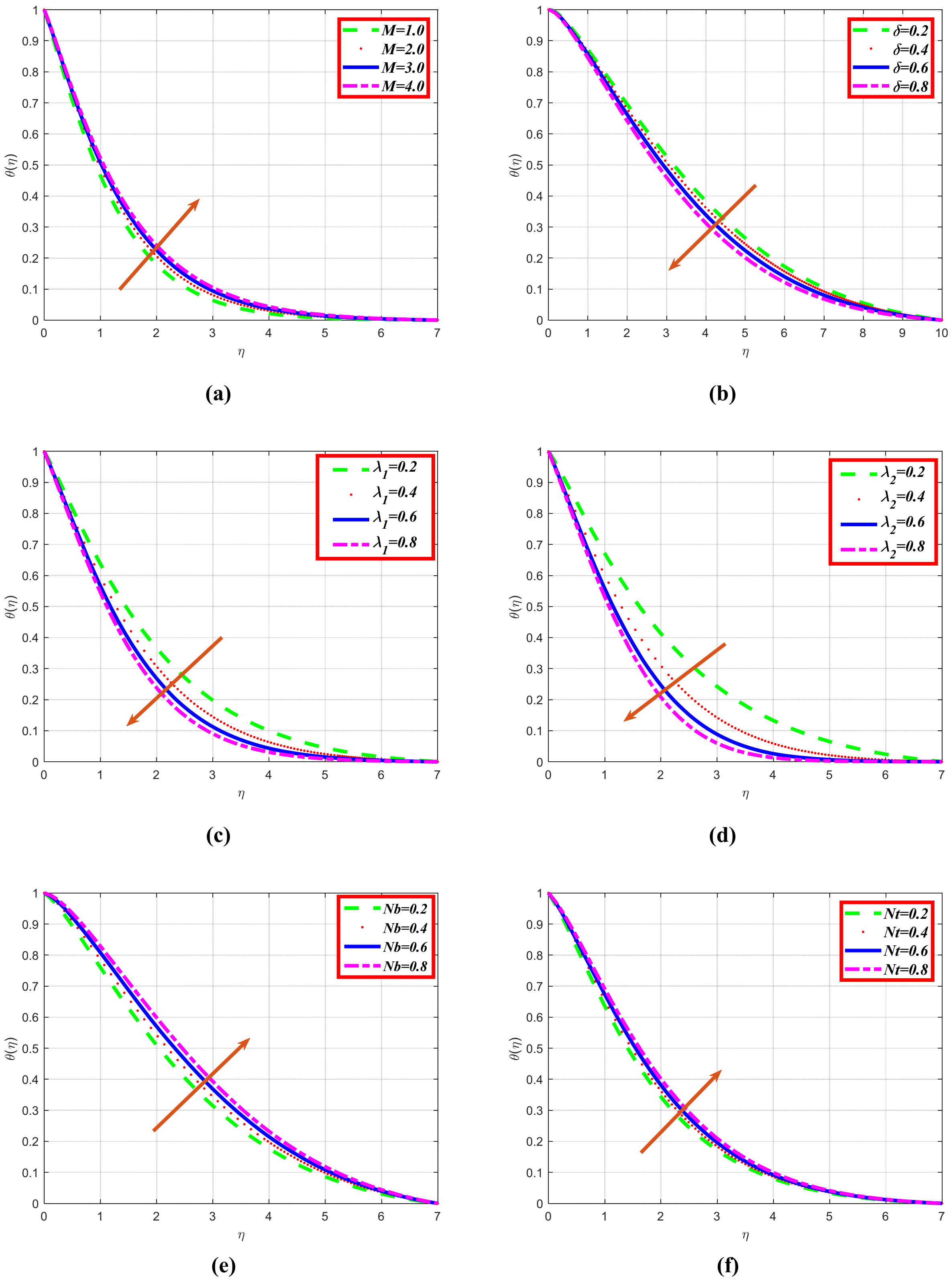

FIGURE 4 | (a–i) Variation of the M, δ, λ_1, λ_2, Nb, Nt, Q, R, and S on the $\theta(\eta)$. [Colour figure can be viewed at wileyonlinelibrary.com]

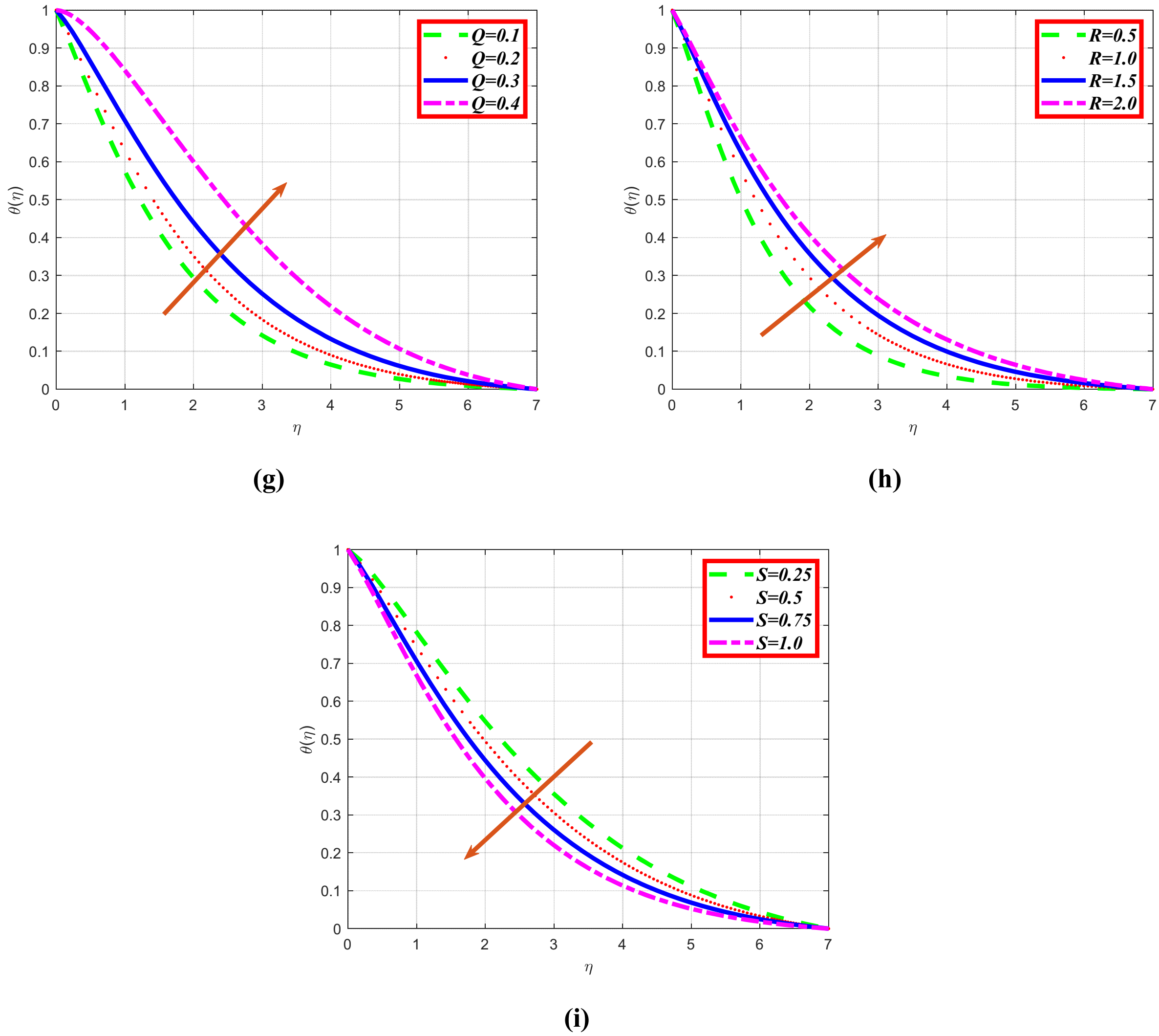

FIGURE 4 | (Continued)

pharmaceutical manufacturing and catalytic power plants, where the amount of reactants is controlled.

Figure 6a,b provides streamlined graphs of a micropolar nanofluid flow pattern for various parameter values. The flow lines in Figure 6a correspond to are for $M = 0.5$ and $K_p = 0.2$. In this context, M denotes the magnetic dimension, whereas K_p signifies the porosity component. The graphic demonstrates that the velocity increases as η increases. The flowing lines in Figure 6b correspond to $K = 0.5$ and $\lambda_1 = 0.1$ where K is a micropolar fluid component and λ_1 is a thermal Grasfof characteristic. The flow trajectory exhibits similarity, demonstrating the influence of these factors on the rotating properties of the medium and the transmission of energy.

The contour visualizations in Figure 7a,b depict the intricate interaction between magnetic impact, permeability, micropolar features, and buoyancy gradients in influencing the thermal behavior of micropolar nanofluids. In Figure 7a, the elevated magnetic coefficient M signifies a stronger magnetism, which may influence the motion of the fluid tiny particles, resulting in fluctuations in heat transmission. The coefficient Kp represents the porousness of the medium, which determines the medium's capacity to allow the movement of fluid and heat via its permeable surface. The micropolar coefficient K describes the micro-rotations and intrinsic movements of the fluid, which impact its general behavior and heat transmission. The buoyant forces caused by thermal variations impact the radiative heat transport inside the fluid, which is influenced by λ_1.

When trying to figure out how much drag a micropolar nanofluid would impose on a surface, skin friction is a key factor to consider, as seen in Table 1. Physiological appliances, microbiological mechanisms, and fabrication procedures are just a few examples of systems that might benefit from this information since it helps to optimize their effectiveness by decreasing drag. Learning about skin friction also aids in improving thermal transfer efficacy and decreasing energy usage in industrial operations. A magnetic field-induced Lorentz force, acts as an obstacle to the flow of fluid, dampening the effects of skin friction and velocity disparities. The uniform velocity disparity at the surface level is reduced when the micropolarity increases the axial viscosity. When applied to porous material, the Darcy–Forchheimer parameter raises the flow barrier and reduces the fluid velocity

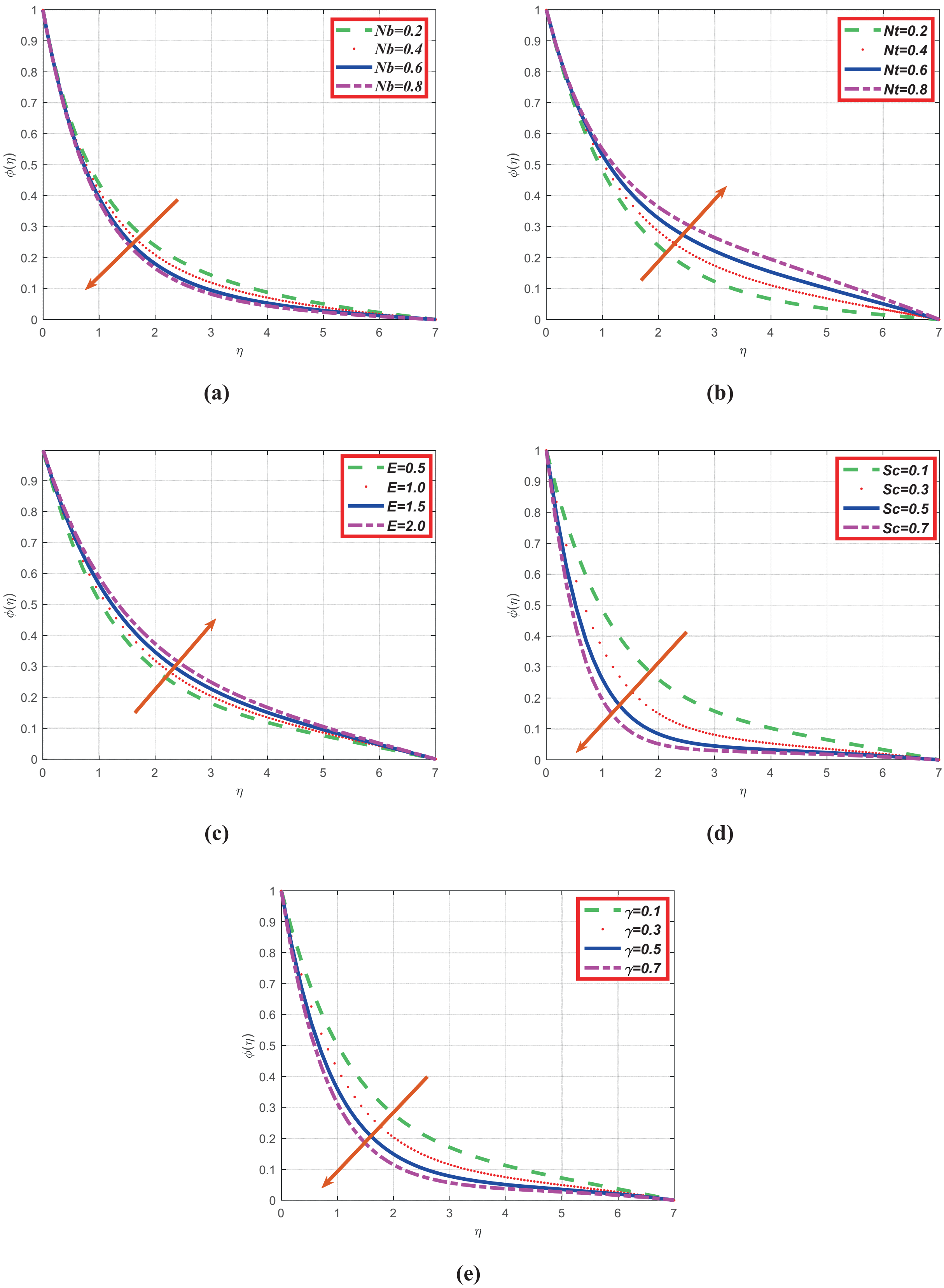

FIGURE 5 | (a–e) Variation of the $Nb, Nt, E, Sc,$ and γ on the $\phi(\eta)$. [Colour figure can be viewed at wileyonlinelibrary.com]

close to the surface. The distribution of velocity at the barrier is reduced as a result of suction removing fluid from the boundary layer. All of these things work together to make surfaces that come into touch with micropolar nanofluids feel less drag. Increased porosity decreases the barrier to flow, resulting in enhanced fluid velocity at the surface and increased skin friction.

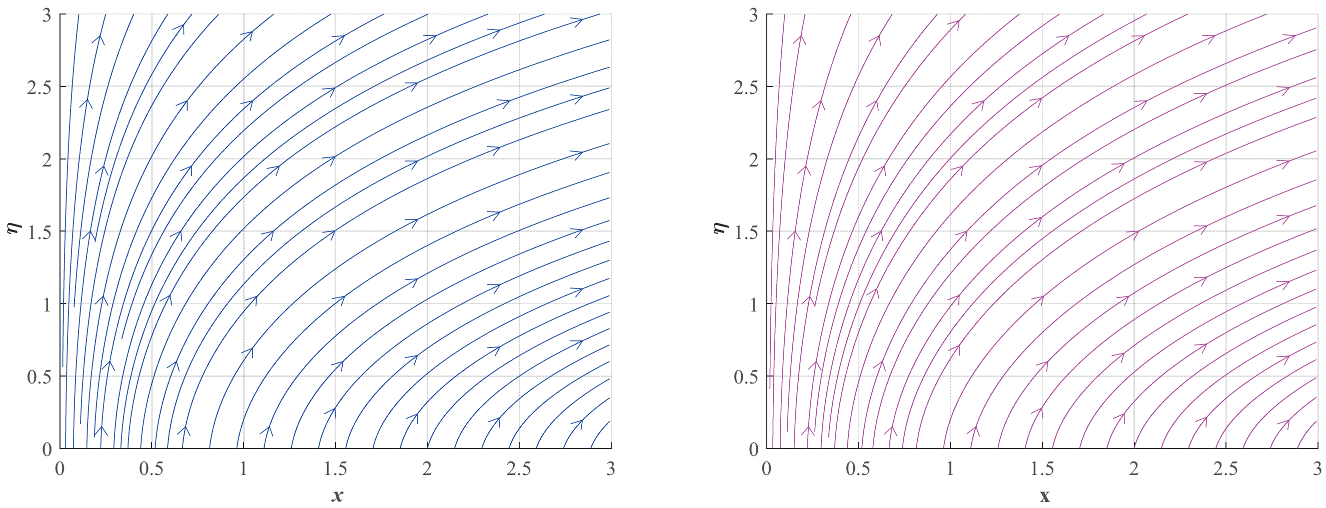

(a) (b)

FIGURE 6 | (a) Streamline plot for $M = 0.5, K_p = 0.2$. (b) Streamline plot for $K = 0.5$, $\lambda_1 = 0.1$. [Colour figure can be viewed at wileyonlinelibrary.com]

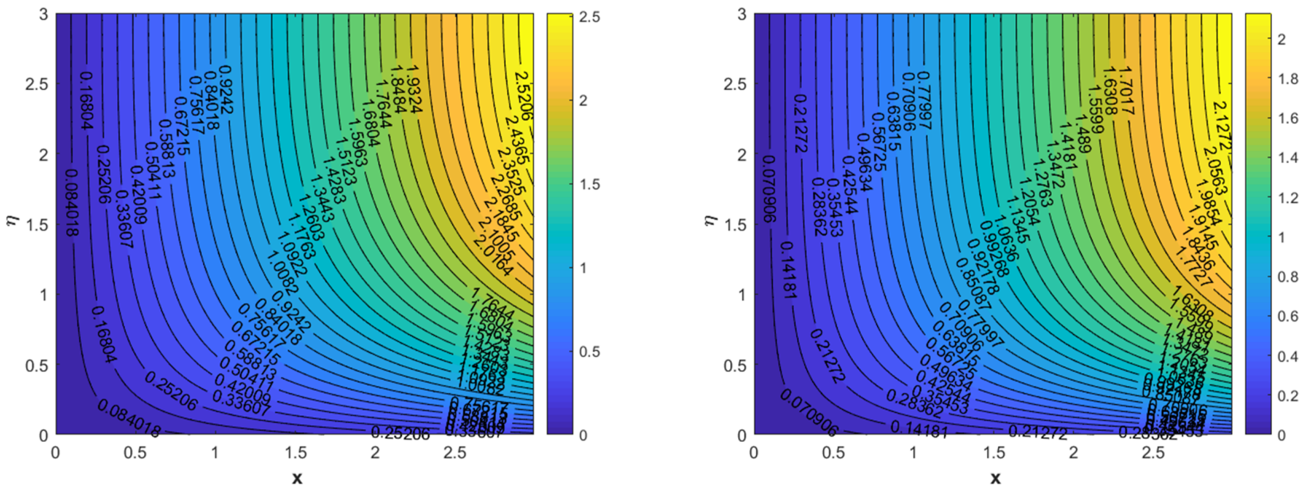

(a) (b)

FIGURE 7 | (a) Contour plot for $M = 0.5, K_p = 0.2$. (b) Contour plot for $K = 0.5$, $\lambda_1 = 0.1$. [Colour figure can be viewed at wileyonlinelibrary.com]

Higher thermal Grashof number amplifies the buoyant forces resulting from temperature disparities, leading to an augmentation in flow rates and velocity variations near the outer layer. Similarly, an increased solutal Grashof count amplifies buoyancy effects resulting from concentration disparities, which in turn enhances the flow and velocity variations, ultimately causing skin friction to rise.

The coupled stress in micropolar flows refers to the coupling within the spinning and axial movements of the fluid, which significantly affects the behavior of the stream. This can be shown in Table 2. Coupled stress in micropolar tiny fluids grows when both thermal and solutal Grashof indices rise. This is due to these factors boosting buoyancy forces, which in turn promote the flow and nanoparticle contact, leading to an upsurge in coupled stress. On the other hand, coupled stress typically falls when the aforementioned parameters—micropolar fluid parameter, Darcy–Forchheimer, porosity, boundary, and suction parameters increase—, stabilizing the rate of flow while reducing its rate and limiting rotational–translational couplings. The coupled stress is reduced because the magnetism generates a Lorentz force that decelerates the velocity of the stream, the micropolar fluid characteristic amplifies the consequences of viscosity, and improved porosity and suction properties make the fluid more stable.

The Nusselt number in micropolar flows shows radiative heat transfer efficacy compared to thermal conductivity (Table 3). Due to higher heat transfer via radiation, larger thermal boundary layers supporting optimal transpiration, and its kinetic translation into heat energy, it rises with radiation attribute, Prandtl number, and Eckert number in micropolar nanofluids. Increased thermal relaxation, Brownian motion, thermophoresis, heat source, and temperature differential characteristics lower the Nusselt number. Thermal relaxation decreases heat transmission, whereas

TABLE 1 | Numerical outcomes of skin friction.

M	K	K_p	Fr	λ_1	λ_2	S	$C_f(Re)^{\frac{1}{2}}$
1.0							−2.960817
2.0							−3.597412
3.0							−4.134997
	0.5						−3.868146
	1.0						−4.210328
	1.5						−4.537820
		1.0					−4.084561
		2.0					−4.563630
		3.0					−4.995754
			0.5				−3.672276
			1.0				−3.853173
			1.5				−4.026047
				0.2			−3.491052
				0.4			−3.284710
				0.6			−3.085128
					0.2		−3.512503
					0.4		−3.342737
					0.6		−3.173214
						0.25	−3.748952
						0.5	−4.015830
						0.75	−4.300484

TABLE 2 | Numerical outcomes of coupled stress.

M	K	Fr	K_p	λ_1	λ_2	m	S	$C_s(Re)^{\frac{1}{2}}$
1.0								−0.733086
2.0								−0.853683
3.0								−0.948316
	0.5							−0.943042
	1.0							−0.996967
	1.5							−1.031723
		0.5						−0.869522
		1.0						−0.907413
		1.5						−0.943159
			1.0					−0.939661
			2.0					−1.019996
			3.0					−1.089540
				0.2				−0.841139
				0.4				−0.811834
				0.6				−0.778566
					0.2			−0.841594
					0.4			−0.815510
					0.6			−0.787076
						0.1		−0.112364
						0.3		−0.481313
						0.5		−0.853683
							0.25	−0.967377
							0.5	−1.186996
							0.75	−1.446719

Brownian motion and thermophoresis disperse nanoparticles, impeding heat transmission. Localized heating from radiant sources and significant variations in temperature generate thermal swaying, reducing convective thermal transfer efficiencies.

The Sherwood number in micropolar fluid flow is a key parameter that quantifies the effectiveness of the conduction of mass compared to distribution. Increased Sherwood numbers indicate increased rates of mass exchange (Table 4). Schmidt number, chemical reaction rate, thermophoresis, and temperature difference factors enhance Sherwood's number in micropolar fluids. Convective mass movement increases with a larger concentration boundary layer and greater Schmidt ratio. Chemical reactions enhance species mobility and mass migration. Temperature swings provide variation in concentration that improves thermal mass transport, whereas thermal analysis moves nanoparticles from hot to cold locations.

5 | Conclusion

This extensive numerical analysis shows that the physical factors controlling the mass transport, heat transfer, and flow properties of MHD micropolar nanofluids interact in a complex and important way. Magical fields, pores, heat, chemical processes, and activation energy were all included in the study. These characteristics have a major effect on the fluid's behavior, which might be used strategically in different engineering contexts. If we want to maximize system performance and energy efficiency in all sorts of technical settings, we need to understand these relationships. The following are the most important takeaways from this investigation, to summarize:

- According to the velocity persona, magnetic fields (M), micropolar fluid features (K), porosity (K_p), and the Darcy–Forchheimer effect (Fr) strongly affects fluid motion, lowering velocity with increasing values. Boundary constraints (m) and suction (S) determine flows and the barrier dimension while heating and solutal Grashof factors control stability and velocity differential.
- The increased Lorentz force, which serves as a physical barrier to the fluid's motion, is the direct cause of the observed decrease in fluid velocity as magnetic field strength (M) increases. Microfluidic devices may use this technique to regulate fluid flow precisely.
- Enhanced microrotation with increased permeability demonstrates the relationship between fluid density and permeability of media, providing insights for the development of innovative filter and separation technologies.
- Increased temperature distributions resulting from enhanced Brownian motion (Nb) and thermophoresis (Nt) are critical for the improvement of thermal conductivity, which is significant for heat exchangers and thermal storage systems.

TABLE 3 | Numerical outcomes of Nusselt number.

R	Pr	δ	Nb	Nt	Ec	Q	α_1	S	$(Re)^{-\frac{1}{2}}\,Nu$
0.5									0.200119
1.0									0.281866
1.5									0.369576
	0.7								0.199916
	0.8								0.201580
	0.9								0.204772
		0.2							0.200119
		0.4							0.199607
		0.6							0.199186
			0.2						0.212377
			0.4						0.188728
			0.6						0.167426
				0.2					0.207685
				0.4					0.192637
				0.6					0.177914
					0.1				0.200119
					0.2				0.096488
					0.3				−0.007161
						0.1			0.200119
						0.2			0.000846
						0.3			−0.312848
							0.1		0.200672
							0.2		0.200119
							0.3		0.199562
								0.25	0.269882
								0.5	0.399020
								0.75	0.543705

- An increase in the Schmidt number (Sc) correlates with a decrease in concentration profiles, signifying improved mass diffusion in comparison to momentum diffusion, which is crucial for optimizing reactants and systems for drug delivery.
- Understanding micropolar nanofluid skin friction helps optimize pharmaceutical components, microorganism systems, and manufacturing. Better heat transmission, less drag, and less energy use result from this knowledge. Increasing porosity and Grashof values impact flow rate, velocity, and skin friction.
- The study indicates that in micropolar nanofluids, the Nusselt number increases due to enhanced radiative heat transfer, which is affected by the radiation characteristic, Prandtl number, and Eckert number.
- Conversely, restrictions on heating, thermophoresis, Brownian motion, and thermal relaxation all work to lower it. In a chemical reaction, the Sherwood number—a measure of mass transfer efficiency—increases when the Schmidt number, quantity of the reaction, thermophoresis, and temperature fluctuations all rise.

TABLE 4 | Numerical outcomes of Sherwood number.

Sc	γ	E	Nb	Nt	α_1	$(Re)^{-\frac{1}{2}}\,Sh$
0.1						0.295262
0.3						0.516494
0.5						0.686750
	0.3					0.575688
	0.5					0.686750
	0.7					0.779062
		0.5				0.617565
		1.0				0.526529
		1.5				0.461419
			0.2			0.699590
			0.4			0.680163
			0.6			0.673444
				0.2		0.670220
				0.4		0.705274
				0.6		0.748093
					0.1	0.658551
					0.2	0.686750
					0.3	0.716850

This study's findings are useful for optimizing thermal management systems in industry. Understanding how magnetic fields, radiation, and chemical reactions affect heat transfer mechanisms in micropolar nanofluids can be used to design more efficient cooling systems for high-heat-flux devices like nuclear reactors and electronic components. Additionally, manipulating fluid flow and heat transfer through porosity, suction, and magnetic field strength allows for the design of advanced materials with tailored thermal properties for aerospace engineering, chemical processing, and energy storage. To optimize physiological appliances, microbiological processes, and manufacturing operations by reducing drag, the research provides insights.

5.1 | Limitations of the Study

Considering the study's shortcomings, real-world settings may be more complicated than the mathematical model's steady-state conditions, incompressible fluid, and constitutive equations for nanofluid behavior. Extending the model to three dimensions may provide more insights than the two-dimensional flow arrangement. Further investigations are required to confirm the findings over a wider variety of situations and fluid characteristics. The particular range of factors tested may further limit the generalizability of the results.

5.2 | Future Scope

The future prospects of this work are investigating innovative nanofluid compositions to enhance heat and mass transport, constructing more accurate models to account for dynamic phenomena, and verifying the results by experimental investigation.

Integrating these insights may boost the effectiveness, reliability, and conserving energy in several areas, including industrial operations like cooling mechanisms and medicines.

Nomenclature

Letters

B_o	uniform magnetic field $\left(\mathrm{kg/S^2A}\right)$
D_B	Brownian diffusion coefficient
D_T	thermophoresis diffusion coefficient
Ec	Eckert number
Fr	Darcy–Forchheimer
K_r	rate of reaction constant
K_p	porosity parameter
K	micropolar fluid parameter
M	magnetic field
m	boundary parameter
Nb	Brownian motion
Nt	thermophoresis parameter
Nu	Nusselt number
Pr	Prandtl number
Q	heat source parameter
R	radiation parameter
S	suction parameter
Sc	Schmidt number
Sh	Sherwood number
T_w	temperature near the sheet (K)
T_∞	free stream temperature (K)

Greek Symbols

λ_1	thermal Grashof number
λ_2	solutal Grashof number
α_1	temperature difference
γ	chemical reaction parameter
δ	thermal relaxation parameter
ρ	fluid density $\left(\mathrm{kg/m^3}\right)$
ρC_p	fluid thermal capacity $\left(\mathrm{J/m^3K}\right)$
υ	kinematic viscosity $\left(\mathrm{m^2/s}\right)$
μ	dynamic viscosity (kg/(ms))

Acknowledgments

All authors are very much grateful to their respective institutes for carrying out the research work.

Conflicts of Interest

The authors declare no conflicts of interest.

Data Availability Statement

All data that support the findings of this study are included in the article.

References

1. S. U. Rehman, A. Mariam, A. Ullah, et al., "Numerical Computation of Buoyancy and Radiation Effects on MHD Micropolar Nanofluid Flow Over a Stretching/Shrinking Sheet With Heat Source," *Case Studies in Thermal Engineering* 25 (2021): 100867, https://doi.org/10.1016/j.csite.2020.100867.

2. A. M. Alqahtani, M. R. Khan, N. Akkurt, V. Puneeth, A. Alhowaity, and H. Hamam, "Thermal Analysis of a Radiative Nanofluid Over a Stretching/Shrinking Cylinder With Viscous Dissipation," *Chemical Physics Letters* 808 (2022): 140133, https://doi.org/10.1016/j.cplett.2022.140133.

3. S. Ullah, G. Saddiq, A. H. Majeed, H. Alotaibi, A. S. Hendy, and M. R. Ali, "Computational Study of Conjugate Heat Transfer and Entropy Generation of Hybrid Nano-Particles in an Enclosure With Solid Block," *Case Studies in Thermal Engineering* 67 (2025): 105822.

4. A. H. Majeed, R. Mahmood, D. Liu, et al., "Effects of Oscillation on Convective Thermal Flow in a Vertical Enclosure Filled by Nanofluid Particles," *Case Studies in Thermal Engineering* 61 (2024): 105133.

5. U. S. Mahabaleshwar, S. M. Sachin, A. B. Vishalakshi, G. Bognar, and B. A. Sunden, "Linear Stability Analysis of Micropolar Nanofluid Flow Across the Accelerated Surface With Inclined Magnetic Field," *International Journal of Numerical Methods for Heat & Fluid Flow* 34, no. 9 (2024): 3515–3541.

6. E. A. Algehyne, S. A. Lone, A. Saeed, and G. Bognár, "Analysis of the Heat Transfer Enhancement in Water-Based Micropolar Hybrid Nanofluid Flow Over a Vertical Flat Surface," *Open Physics* 22, no. 1 (2024): 20230201.

7. M. Vinodkumar Reddy and P. Lakshminarayana, "Cross-Diffusion and Heat Source Effects on a Three-Dimensional MHD Flow of Maxwell Nanofluid Over a Stretching Surface With Chemical Reaction," *European Physical Journal Special Topics* 230 (2021): 1371–1379, https://doi.org/10.1140/epjs/s11734-021-00037-9.

8. T. Hayat, Z. Abbas, and T. Javed, "Mixed Convection Flow of a Micropolar Fluid Over a Non-Linearly Stretching Sheet," *Physics Letters A* 372, no. 5 (2008): 637–647, https://doi.org/10.1016/j.physleta.2007.10.086.

9. A. Dawar, Z. Shah, P. Kumam, et al., "Chemically Reactive MHD Micropolar Nanofluid Flow With Velocity Slips and Variable Heat Source/Sink," *Scientific Reports* 10, no. 1 (2020): 20926, https://doi.org/10.1038/s41598-020-77867-y.

10. S. E. Awan, M. A. Z. Raja, F. Gul, Z. A. Khan, A. Mehmood, and M. Shoaib, "Numerical Computing Paradigm for Investigation of Micropolar Nanofluid Flow Between Parallel Plates System With Impact of Electrical MHD and Hall Current," *Arabian Journal for Science and Engineering* 46 (2021): 645–662, https://doi.org/10.1007/s13369-020-05006-7.

11. M. Waseem, M. Jawad, S. Naeem, et al., "Regression Analysis of Cattaneo–Christov Heat and Thermal Radiation on 3D Darcy Flow of Non-Newtonian Fluids Induced by Stretchable Sheet," *Case Studies in Thermal Engineering* 61 (2024): 104959.

12. A. H. Majeed, D. Liu, A. R. Ali, H. Alotaibi, Z. J. Yin, and R. H. Yi, "Numerical Simulations of Energy Storage Performance in a Close Configuration: A Galerkin Finite Element-Based Computation," *Alexandria Engineering Journal* 104 (2024): 56–65.

13. M. Waseem, E. A. Algehyne, N. O. Al-Atawi, G. Bognár, M. Jawad, and S. Naeem, "Non-Similar Analysis of Suction/Injection and Cattaneo-Christov Model in 3D Viscoelastic Non-Newtonian Fluids Flow due to Riga Plate: A Biological Applications," *Alexandria Engineering Journal* 103 (2024): 121–136.

14. M. ur Rahman, F. Haq, M. I. Khan, and M. S. Nawaz, "Irreversibility Analysis in Viscous Nanomaterial Flow With Darcy–Forchheimer and Activation Energy," *International Journal of Applied and Computational Mathematics* 8, no. 6 (2022): 270, https://doi.org/10.1007/s40819-022-00755-4.

15. E. E. Bafe, M. D. Firdi, and L. G. Enyadene, "Magnetohydrodynamic Thermo-Bioconvective Flow of 3D Rotating Williamson Nanofluid With Arrhenius Activation Energy in a Darcy–Forchheimer Medium Over an Exponentially Stretching Surface," *International Journal of Thermofluids* 21 (2024): 100585, https://doi.org/10.1016/j.ijft.2023.100585.

16. L. Ali, Z. Ullah, M. Boujelbene, et al., "Wave Oscillations in Thermal Boundary Layer of Darcy-Forchheimer Nanofluid Flow Along Buoyancy-Driven Porous Plate Under Solar Radiation Region," *Case Studies in Thermal Engineering* 54 (2024): 103980, https://doi.org/10.1016/j.csite.2024.103980.

17. H. Al-Shammari, Z. Ullah, Y. M. Mahrous, et al., "Arrhenius Activation Energy and Thermal Radiation Effects on Oscillatory Heat-Mass Transfer of Darcy Forchheimer Nanofluid Along Heat Generating Cone," *Case Studies in Thermal Engineering* 57 (2024): 104294, https://doi.org/10.1016/j.csite.2024.104294.

18. B. K. Sharma and R. Gandhi, "Combined Effects of Joule Heating and Non-Uniform Heat Source/Sink on Unsteady MHD Mixed Convective Flow Over a Vertical Stretching Surface Embedded in a Darcy-Forchheimer Porous Medium," *Propulsion and Power Research* 11, no. 2 (2022): 276–292, https://doi.org/10.1016/j.jppr.2021.11.005.

19. M. Hasanuzzaman, S. Akter, S. Sharin, M. M. Hossain, A. Miyara, and M. A. Hossain, "Viscous Dissipation Effect on Unsteady Magneto-Convective Heat-Mass Transport Passing in a Vertical Porous Plate With Thermal Radiation," *Heliyon* 9, no. 3 (2023): e14614, https://doi.org/10.1016/j.heliyon.2023.e14614.

20. W. D., Alamirew, G. A. Zergaw, and E. H. Gorfie, "Effects of Hall, Ion Slip, Viscous Dissipation and Nonlinear Thermal Radiation on MHD Williamson Nanofluid Flow Past a Stretching Sheet," *International Journal of Thermofluids* 22: 100646.

21. K. Malleswari, J. M. Nath, M. V. Reddy, M. S. Mala, and B. Dey, "Thermal Performance of Cattaneo-Christov Heat Flux in MHD Radiative Flow of Williamson Nanofluid Containing Motile Microorganisms and Arrhenius Activation Energy," *Journal of Computational and Theoretical Transport* 54, no. 1 (2024): 45–67.

22. S. Alao, S. O. Salawu, R. A. Oderinu, A. A. Oyewumi, and E. I. Akinola, "Investigation of Thermal Radiation and Viscous Heating Effects on the Hydromagnetic Reacting Micropolar Fluid Species Flowing Past a Stretchy Plate in Permeable Media," *International Journal of Thermofluids* 22 (2024): 100600, https://doi.org/10.1016/j.ijft.2024.100600.

23. C. Cattaneo, "Sulla conduzione del calore," *Atti del Seminario Matematico e Fisico Della Università di Modena* 3 (1948): 83–101.

24. C. I. Christov, "On Frame Indifferent Formulation of the Maxwell–Cattaneo Model of Finite-Speed Heat Conduction," *Mechanics Research Communications* 36, no. 4 (2009): 481–486, https://doi.org/10.1016/j.mechrescom.2009.06.006.

25. W. Ibrahim and G. Gadisa, "Finite Element Solution of Nonlinear Convective Flow of Oldroyd-B Fluid With Cattaneo-Christov Heat Flux Model Over Nonlinear Stretching Sheet With Heat Generation or Absorption," *Propulsion and Power Research* 9, no. 3 (2020): 304–315, https://doi.org/10.1016/j.jppr.2020.01.001.

26. H. Waqas, M. Fida, D. Liu, U. Manzoor, and T. Muhammad, "Numerical Simulation of Entropy Generation for Nanofluid With the Consequences of Thermal Radiation and Cattaneo-Christov Heat Flux Model," *International Communications in Heat and Mass Transfer* 137 (2022): 106293, https://doi.org/10.1016/j.icheatmasstransfer.2022.106293.

27. M. B. Ashraf, A. Tanveer, and S. Ulhaq, "Effects of Cattaneo-Christov Heat Flux on MHD Jeffery Nanofluid Flow Past a Stretching Cylinder," *Journal of Magnetism and Magnetic Materials* 565 (2023): 170154, https://doi.org/10.1016/j.jmmm.2022.170154.

28. M. Azam, W. A. Khan, and M. K. Nayak, "Three-Dimensional Flow of Cross Nanofluid Over Bidirectional Moving Surface in Darcy-Forchheimer Medium With Cattaneo-Christov Heat Flux," *Case Studies in Thermal Engineering* 49 (2023): 103250, https://doi.org/10.1016/j.csite.2023.103250.

29. S. Karthik, D. Iranian, and Q. M. Al-Mdallal, "Numerical Simulation of Magneto-Hydrodynamic Fluid Flow With Heat Sink, Chemical Diffusion, and Powell Eyring Fluid Behavior Using Cattaneo–Christov Source Term," *International Journal of Thermofluids* 22 (2024): 100616, https://doi.org/10.1016/j.ijft.2023.100616.

30. M. I. Khan, A. Alsaedi, S. Qayyum, T. Hayat, and M. I. Khan, "Entropy Generation Optimization in Flow of Prandtl–Eyring Nanofluid With Binary Chemical Reaction and Arrhenius Activation Energy," *Colloids and Surfaces A: Physicochemical and Engineering Aspects* 570 (2019): 117–126, https://doi.org/10.1016/j.colsurfa.2019.04.034.

31. M. S. Ram, M. D. Shamshuddin, and K. Spandana, "Numerical Simulation of Stagnation Point Flow in Magneto Micropolar Fluid Over a Stretchable Surface Under the Influence of Activation Energy and Bilateral Reaction," *International Communications in Heat and Mass Transfer* 129 (2021): 105679, https://doi.org/10.1016/j.icheatmasstransfer.2021.105679.

32. T. Salahuddin, A. Maqsood, M. Awais, M. Khan, and M. Altanji, "Significance of MHD Cross Nanofluid Analysis Near a Stretched Surface With Double Stratification and Activation Energy," *International Communications in Heat and Mass Transfer* 143 (2023): 106732, https://doi.org/10.1016/j.icheatmasstransfer.2022.106732.

33. M. Y. Ali, M. Rahman, M. M. Ali, S. F. Ahmmed, and S. Haque, "Data Analysis of Non-Linear Radiative Electro-Periodic MHD Flow Past a Stretching Sheet With Activation Energy Impact," *International Communications in Heat and Mass Transfer* 155 (2024): 107572, https://doi.org/10.1016/j.icheatmasstransfer.2024.107572.